NMR microscopy of pore-space backbones in rock, sponge, and sand in comparison with random percolation model objects

A. Klemm, H.-P. Müller, and R. Kimmich
Universität Ulm, Sektion Kernresonanzspektroskopie, 89069 Ulm, Germany
(Received 22 October 1996)

Two- and three-dimensional ''random swiss-cheese percolation'' and ''random-site percolation'' pore networks were simulated on a computer. The results were used as templates for the fabrication of model objects. The flow of water through the pore spaces of these objects was studied with the aid of NMR microscopy in the velocity-mapping variant. Up to three spatial dimensions and three dimensions for the three velocity components were examined. The results for the model objects were juxtaposed to those for lacunar materials such as pumice, sponge, sand, and glass bead agglomerates. Parameters characterizing the structure were evaluated from conventional NMR images of the water-filled pore spaces. The percolation backbone was determined by eliminating all voxels with velocities below the noise level. [S1063-651X(97)02504-X]

PACS number(s): 47.55.Mh, 87.59.Pw, 61.43.Hv, 47.53.+n

I. INTRODUCTION

Lacunar materials and systems such as pumice, sponge, sand, and glass bead agglomerates form interconnected pore spaces which permit transport of fluids through the samples. It is therefore of interest to establish a set of parameters suitable for the characterization of the geometrical properties of the pore spaces. This requires the development of experimental procedures for the reliable determination of these quantities.

In order to test the possibilities NMR microscopy offers in this respect, predictions of the standard percolation theory [1] were already compared with experimental results in our previous work [2–4]. Random-site percolation clusters were simulated on a computer. The patterns produced in this way were used as templates for the fabrication of two- or three-dimensional lacunar objects. The pore spaces were filled with water and examined with the aid of NMR microscopy techniques. A suitable algorithm for the evaluation of the image data was developed and shown to reliably reproduce the theoretical parameters by which the simulated clusters are characterized.

Random-site percolation networks are well defined and easy to simulate. However, they are less suitable for modeling pore spaces in lacunar systems and granular materials of a practical nature. In this paper we are therefore referring to so-called ''swiss-cheese'' models [5–7] which promise to take the highly branched pore spaces of practical systems better into account. Swiss-cheese percolation models in this context are defined as a uniform transport medium with randomly placed spherical ''voids'' [8]. That is, each ''void'' forms an obstacle for transport of matter. In the present study, the pore space is thus defined as the space complementary to that occupied by the ''void'' distribution.

Corresponding computer simulations were evaluated in terms of fractal parameters. Real swiss-cheese model objects were then composed using the computer-simulated pore-space patterns as templates. The experimental NMR investigation was carried out in analogy to our previous studies of random-site percolation objects [2].

The class of systems to be compared with the model objects is called ''lacunar'' [9]. In the present study, this includes samples of natural origin such as natural sponge, pumice stone, and agglomerates of granular materials such as glass beads or quartz sand. Apart from structural properties, transport phenomena were examined using a velocity-mapping NMR technique. Transport, of course, refers to percolation features of utmost practical relevance [7]. The transport-limiting structure is termed the ''percolation backbone.''

In suitable cases, the pore space of lacunar media can be characterized by scaling laws with well-defined exponents [1,10–15]. Parameters of particular interest are the fractal (or pseudofractal) dimension d_f, the correlation length ξ, the percolation probability P_∞, and the fractal (or pseudofractal) dimension of the backbone d_f^b. In the following, experimental determinations of such parameters with the aid of NMR microscopy techniques will be discussed and examined with respect to the potential distinction of the pore spaces of different materials on this basis.

II. EXPERIMENTAL SECTION

Random-site and swiss-cheese percolation model objects were fabricated. The random-site percolation clusters based on computer simulations such as displayed in Fig. 1 were composed of stacks of 0.5 mm thick polystyrene disks. These disks were milled with the aid of a LPKF (Leiterplatten-Konturfräsen) circuit board plotter using computer-simulated templates as described in [2,3]. The cubic basis of the cluster lattice was 32 lattice constants wide in each space direction. The cross sections of the pores were quadratic with an edge length of 0.5 mm.

The swiss-cheese percolation cluster objects were rebuilt according to computer simulations such as those represented in Fig. 2. The objects were constructed in the form of stacks of 0.3 mm thick polystyrene disks. Figures 3(a) and 3(b) show photographs of complete two- or three-dimensional swiss-cheese objects.

The basis of the clusters was again cubic. In the two-dimensional case, the extension of the cluster was 80 lattice

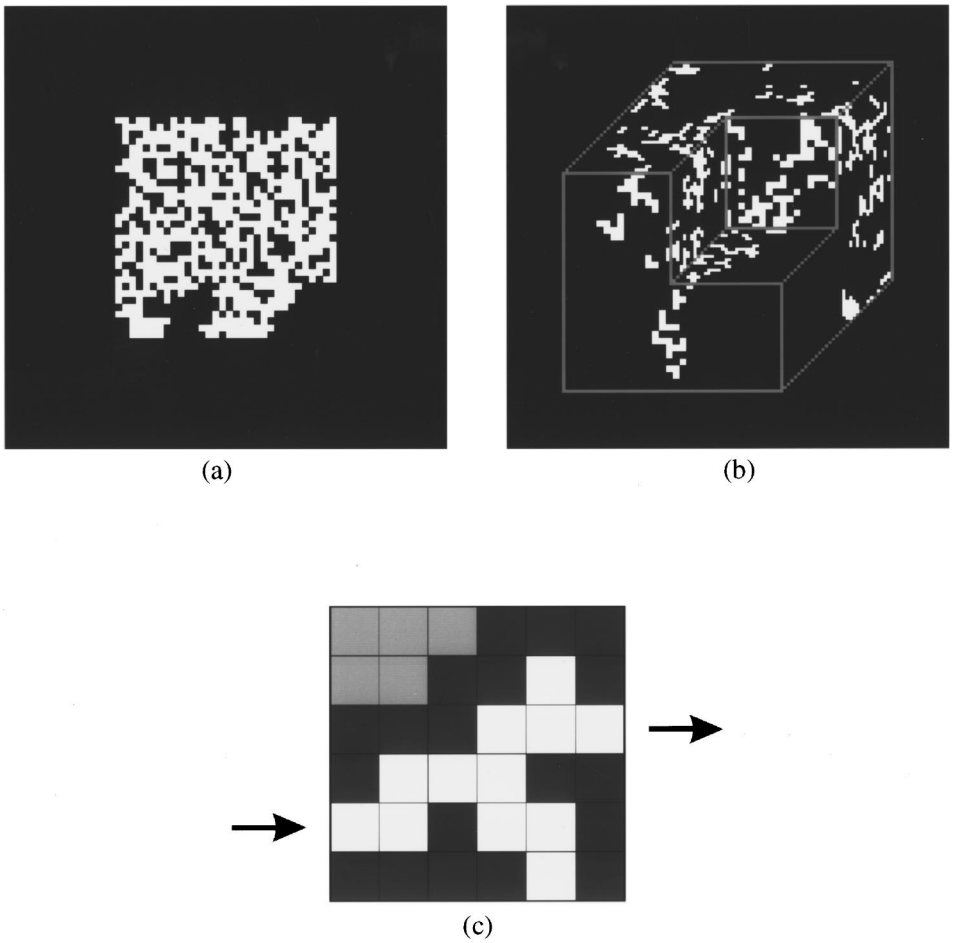

FIG. 1. Computer-simulated site percolation networks with lattice sizes of 32×32 and $32\times32\times32$ lattice points in two and three Euclidean dimensions, respectively. Any isolated clusters were eliminated. The white voxels represent the pore space. (a) $d_E=2$, $p-p_c=0.060$. (b) $d_E=3$, $p-p_c=0.035$ (multisectional view of the voxels located on the surfaces). (c) Schematic illustration of the pore structure: white, interconnected pore space; gray, isolated cluster; black, matrix.

constants in each space direction. The three-dimensional objects comprised 64 lattice constants in each direction. The edge length of the quadratic cross sections of the pores was 0.3 mm.

The NMR microscopy pulse schemes used in this work were optimized for imaging of liquids. The NMR signal of the polystyrene material therefore was negligible compared with the signal of the water filled into the pore spaces. Before injecting water, the pore spaces were evacuated in order to avoid air bubbles which tend to block the dead ends of the pore space. Magnetic field inhomogeneities in the field of view were less than ±0.015 ppm as detected by magnetic resonance spectroscopic imaging (e.g., Ref. [16]).

The proton magnetic resonance imaging experiments were carried out with a Bruker Biospec 47/40 magnet (4.7 T) combined with a partly home-made radio frequency (rf) unit. The maximum gradients were 0.6 T/m. Typical gradient switching times were 0.2 ms.

Two- or three-dimensional (proton) spin-density image data were recorded using a gradient-recalled echo pulse sequence for the spatial encoding (upper part of Fig. 4). The digital resolution varied from 0.10 mm to 0.30 mm. The sample dimensions ranged from 8 mm to 20 mm. The local spin density is equivalent to the local porosity of the material, where ''local'' refers to the two-dimensional pixel or three-dimensional voxel at the considered position.

Based on bipolar field gradient pulses, the Fourier encoding velocity imaging (FEVI) principle [17,18] permits phase encoding of the gradient echo proportional to the local velocity component along the respective field gradient direction. In this way, maps of the velocity vector of water percolating through the pore space can be acquired. The radio frequency and field gradient pulse sequence is shown in Fig. 4. More detailed information on this method can be found in [19,20].

The absolute value of the local flow velocity $v=\sqrt{v_x^2+v_y^2+v_z^2}$ was then calculated from the three velocity components which were separately measured with the aid of this pulse sequence.

The image data sets recorded in this way were up to six dimensional. On this basis, any two- or three-dimensional representation of the local spin density or the local velocity components or the local velocity magnitude can be rendered in principle. Spin-density images mirror the full percolation cluster, whereas the percolation backbone can be identified with the aid of the velocity data.

III. CHARACTERISTIC PARAMETERS IN PERCOLATIONTHEORY

The porosity of a lacunar percolation system is defined by

$$\rho=\frac{V_p}{V_p+V_m}, \tag{1}$$

where V_p is the total pore volume, and V_m is the total matrix volume without pores in the sample fraction under consideration. We distinguish the ''overall porosity'' referring to the

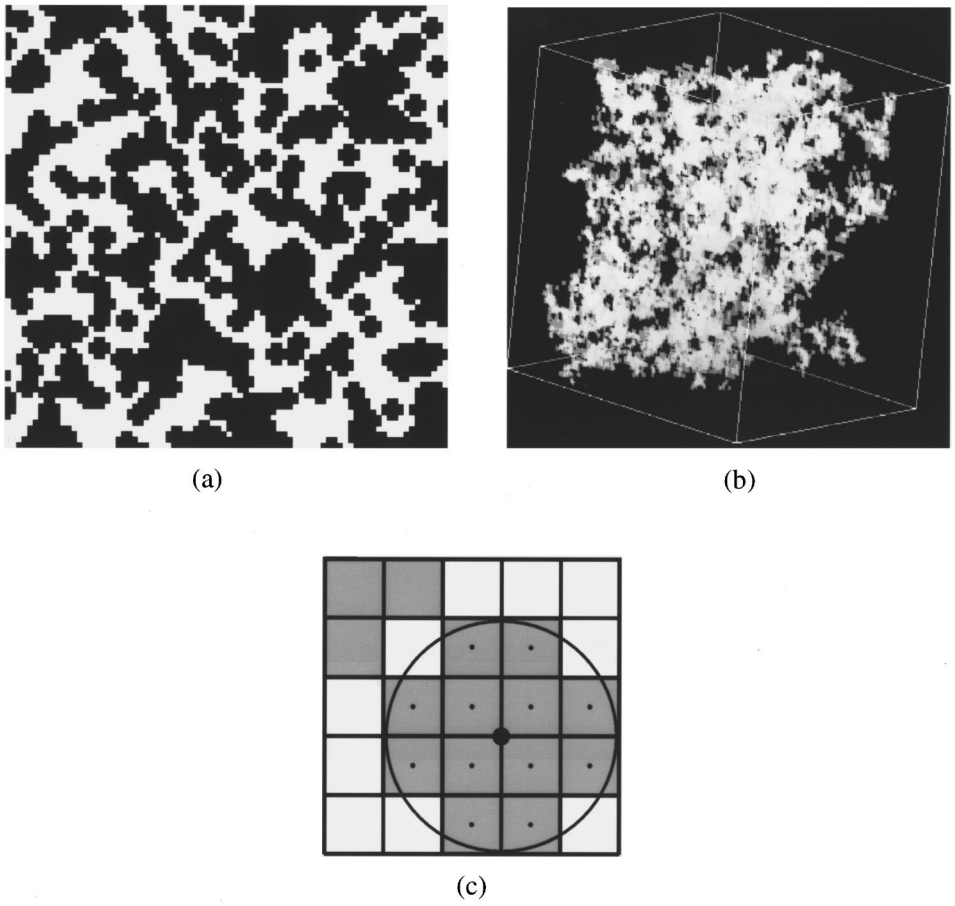

FIG. 2. Computer-simulated swiss-cheese percolation networks with lattice sizes of 80×80 and $64\times64\times64$ lattice points in two and three Euclidean dimensions, respectively. Any isolated clusters were eliminated. The white voxels represent the pore space. (a) $d_E=2$, $p-p_c=0.087$. (b) $d_E=3$, $p-p_c=0.009$ (projection of the total pore space on the drawing plane; the gray shades of the three-dimensional black-and-white data set arise from the superposition of voxel projections). (c) Schematic illustration of the approximate representation of spherical transport medium ''voids'' (percolation obstacles) by a finite number of discrete matrix voxels. In the two-dimensional case shown here, the circle comprises the same area as the pixels marked by dots.

whole sample, and the ''local porosity'' characterizing the situation within a voxel at a certain position.

In the NMR imaging experiments to be described in the following, the pores were completely filled with water. The local porosity $\rho=\rho(\mathbf{r})$ is then equal to the local water spin density, that is, the volume fraction of the water in the voxel under consideration. Therefore the amplitude of the water signal of a voxel is directly proportional to the porosity in this voxel.

The average porosity of the whole sample can be determined from the masses of the dry matrix material (m_m) and the fluid-filled sample (m_w+m_m) according to

$$\overline{\rho_0}=\frac{m_w}{m_w+q_r\,m_m}, \tag{2}$$

where q_r is the ratio of the mass densities of the fluid and the matrix material.

The theory of random percolation networks suggests a scaling window of self-similarity in the range $a<r<\xi$, where a is the structure-forming elementary length, and ξ the correlation length. Percolation clusters in this range have a volume-averaged density varying with the probe-volume radius according to [1]

$$\rho_V(r)\propto\begin{cases} r^{d_f-d_E}, & a<r<\xi \\ P_\infty, & r>\xi. \end{cases} \tag{3}$$

The Euclidean dimension is denoted by d_E, the fractal dimension by d_f. The fractal dimensions of two- and three-dimensional random-site percolation networks are found to be [1] $d_f=1.9$ in $d_E=2$ and $d_f=2.5$ in $d_E=3$ (see also Fig. 10). The percolation probability, P_∞ is a constant (P_∞ corresponds to $\overline{\rho_0}$ of real samples).

Random-site percolation networks are defined by a certain occupation probability of the sites, p, and the threshold value p_c. In the vicinity of p_c and for $p>p_c$, the parameters P_∞ and ξ obey [1]

$$P_\infty\propto(p-p_c)^\beta, \tag{4}$$

$$\xi\propto(p-p_c)^{-\nu}. \tag{5}$$

The exponents of the above power laws are related with each other according to [1]

$$d_f=d_E-\frac{\beta}{\nu}. \tag{6}$$

A severe problem arising with evaluations of data obtained in real experiments such as NMR imaging studies is that the systems are unavoidably restricted to relatively small cluster sizes and ensembles. It was therefore essential to develop evaluation procedures coping with such limitations [2]. The power law given in Eq. (3), for instance, can be tested by determining the mean volume-averaged porosity as a function of the radius r of the probe volume. A suitable evaluation method is the so-called ''sandbox'' method [10]:

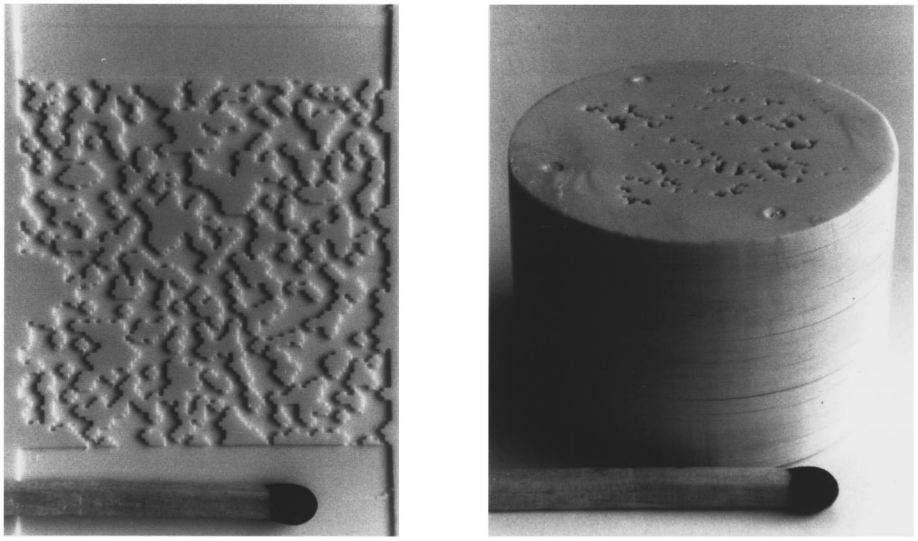

(a) (b)

FIG. 3. Photographs of two- and three-dimensional swiss-cheese percolation objects examined in this study. In each case the pore space was first simulated on a computer and then machined using the computer results as templates. The matches on the bottom illustrate the length scale. (a) Two-dimensional network milled into a polystyrene plate with a thickness of 0.5 mm. The size is 24×24 mm^2. (b) Three-dimensional object composed of 64 polystyrene disks of a thickness of 0.3 mm each. The cross-sectional area of the three-dimensional percolation cluster was 20×20 mm^2.

$$\overline{\rho_V}(r)=\frac{1}{N_p}\sum_{i=1}^{N_p}\frac{1}{N_v}\sum_{j=1}^{N_v}\rho(\mathbf{r}_j)\quad(|\mathbf{r}_i-\mathbf{r}_j|\leqslant r),\tag{7}$$

where

$$\rho(\mathbf{r}_j)=\begin{cases}0 & (\text{site }\mathbf{r}_j\text{ not occupied})\\ 1 & (\text{site }\mathbf{r}_j\text{ occupied}).\end{cases}\tag{8}$$

The quantity N_v is the number of voxels in the probe volume. The center of the probe volume must be at a position $\mathbf{r}_i$ belonging to the considered cluster. The condition $|\mathbf{r}_i-\mathbf{r}_j|\leqslant r$ is the consequence of the spherical shape of the probe volume. The expression in Eq. (7) finally refers to the ensemble mean value of N_p probe volumes of equal size.

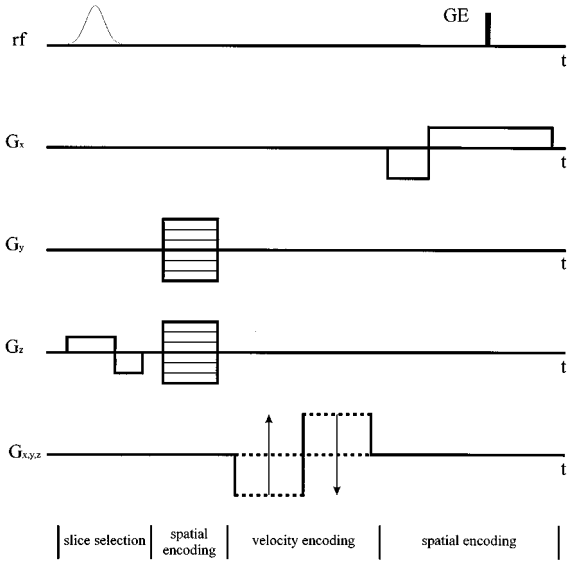

FIG. 4. Radio frequency (rf) and field gradient (G_i, $i=x,y,z$) pulse scheme of the NMR microscopy techniques employed in this study (see Sec. II). The sequence is based on gradient-recalled echoes (GE). The three-dimensional spatial encoding is performed with the aid of two phase-encoding and one frequency-encoding gradient. The three velocity components are phase encoded with the aid of bipolar gradient pulses (bottom line). For details see Ref. [20], for instance.

IV. COMPUTER SIMULATIONS

A. Random-site percolation networks

The percolation objects used for the NMR experiments are based on computer simulations of random percolation clusters which served as templates for the object fabrication. The computer simulations of random percolation networks

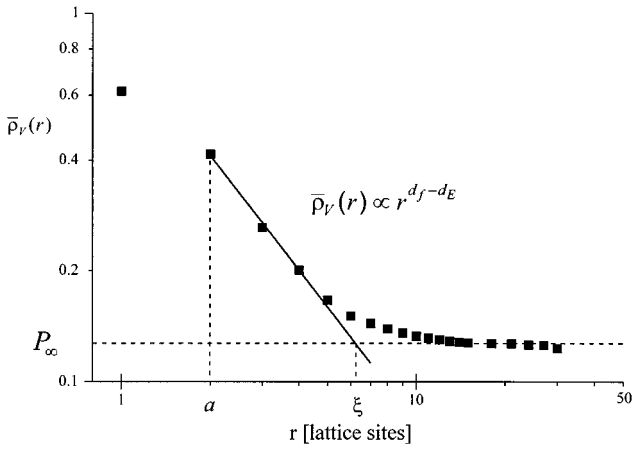

FIG. 5. Mean volume-averaged porosity $\overline{\rho_V}(r)$ as a function of the probe-volume radius r. The data were evaluated from the computer-simulated three-dimensional swiss-cheese percolation network shown in Fig. 2(b). The shortest radius a, i.e., the structure-forming elementary length, of the probe-volume comprising at least one sphere of the matrix is equal to two lattice constants as becomes obvious from Fig. 2(c). Smaller probe volume radii outside the scaling window lead to reduced mean volume-averaged porosities which are not characteristic for the fractal properties of the cluster.

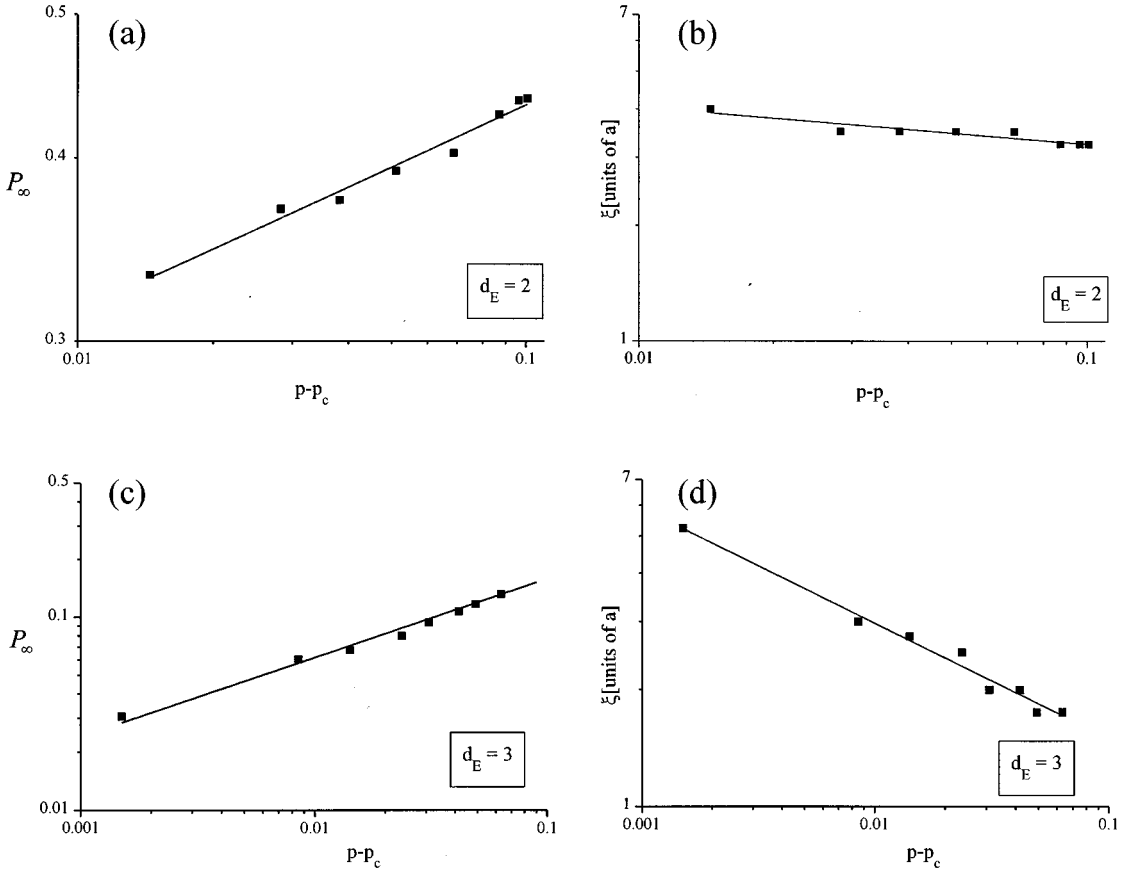

FIG. 6. Verification of the proportionalities $P_\infty \propto (p-p_c)^\beta$ and $\xi \propto (p-p_c)^{-\nu}$ on the basis of computer simulations of two- and three-dimensional swiss-cheese percolation networks. The correlation length ξ is displayed in units of the disk or sphere radius a. (a) $\beta=0.14$ (fixed literature value) $\rightsquigarrow p_c=0.35$. (b) $\nu=0.24$ [value fitted using the threshold value of (a)]. (c) $\beta=0.41$ (fixed literature value) $\rightsquigarrow p_c=0.074$. (d) $\nu=0.30$ [value fitted using the threshold value of (c)].

were carried out assuming the same spatial resolution relative to the object size as in the experiments, that is, a digital resolution of either 0.30 mm or 0.25 mm. Since the computer-simulated patterns were to be used as templates for the fabrication of real objects, only three-dimensional patterns that consist of two-dimensional slices without ''islands'' were considered.

The site percolation clusters were composed on a cubic lattice with the aid of the random-number generator of the Borland C programming language. Each site of the lattice is occupied randomly with the probability p. The occupation of two neighboring lattice sites is interpreted as a passage. Above the percolation threshold p_c ($p_c=0.5927$ for $d_E=2$ and $p_c=0.3116$ for $d_E=3$ [1]) one largest cluster exists connecting opposite edges of the network [see the ''white'' clusters in Figs. 1(a) and 1(b), for instance]. The NMR imaging resolution was chosen in such a way, that each cluster site is probed by four NMR imaging pixels in two-dimensional clusters or eight voxels in three dimensions. The elimination of isolated clusters led to the desired network [Fig. 1(c)]. Thus the network size that can be examined in the NMR microscopy experiments is restricted to $32\times32\times32$ lattice sites for practical reasons [2].

B. Swiss-cheese percolation networks

The swiss-cheese model to be considered here is defined by randomly distributed spherical obstacles in a uniform transport medium [8]. In this case, the percolation thresholds are found to be $p_c=0.32$ for $d_E=2$ and $p_c=0.032$ for $d_E=3$ [5,13,21]. The networks were based on quadratic or cubic lattices for the two- or three-dimensional cases, respectively. ''Disks'' or ''spheres'' with radii of two lattice con-

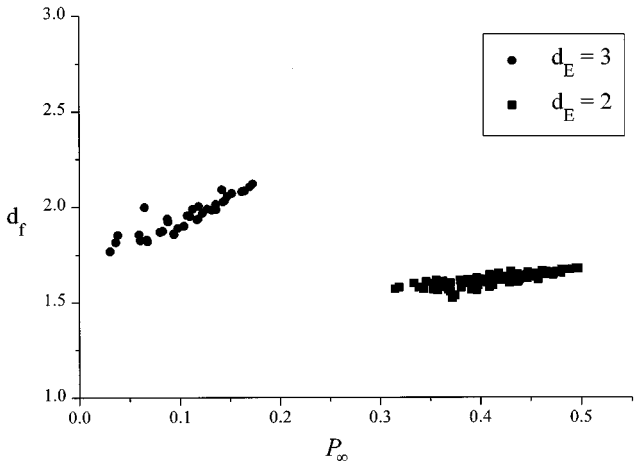

FIG. 7. Fractal dimension d_f as a function of the percolation probability P_∞. The data were evaluated from computer-simulated swiss-cheese percolation networks. Lattice sizes: 128×128 ($d_E=2$) and $64\times64\times64$ ($d_E=3$).

TABLE I. Parameters of random percolation clusters as determined in this work (SP, site percolation; SC, swiss cheese; *c*, computer simulated; *e*, experimental data from NMR data sets).

	$d_E=2$				$d_E=3$			
	p_c	P_∞	d_f	d_f^b	p_c	P_∞	d_f	d_f^b
SP;*c* [a]	0.5927	0.5–0.6	1.89	1.6–1.8	0.3116	0.2–0.3	2.53	1.9
SP;*e* [a]		0.5–0.6	1.9	1.6–1.8		0.2–0.3	2.5	2.2-2.3
SC;*c*	0.37	0.3–0.5	1.55–1.68		0.080	0.03–0.2	1.8–2.1	
SC;*e*		0.3–0.4	1.60–1.69	1.48–1.55		0.06–0.2	1.8–2.0	1.7–1.9

[a]Data from [2].

stants were placed on the lattices at random. The actual volume covered by these objects is determined by the finite resolution of the lattice, and is indicated in black in Figs. 2(a) and 2(b), for instance.

A passage is defined by two ''white'' pixels or voxels touching each other at least at one corner [Fig. 2(c)]. For practical reasons, the cluster size was limited to 80×80 [Fig. 2(c)] and $64\times64\times64$ [Fig. 2(b)] lattice sites in two and three dimensions, respectively.

The porosity of the network can be determined as the ratio of ''white'' (i.e., pore space) pixels or voxels and the total number of lattice sites. In the three-dimensional case, it is also described by

$$\rho_n=\exp(-\tfrac{4}{3}\pi nR^3), \tag{9}$$

where n is the number density of spheres, and R is the radius of the spheres [22,23]. The corresponding expression for two-dimensional networks is

$$\rho_n=\exp(-\pi nR^2). \tag{10}$$

In this case, ρ_n represents the fraction of ''white'' lattice sites, that is, it is analogous to the occupation probability of the site percolation networks.

The fractal parameters are again determined from the volume-averaged porosity $\overline{\rho_V}(r)$ as a function of the probe-volume radius (Fig. 5, for instance). Differences to the values considered to be universal in all random percolation networks are due to the finite and discrete lattice approach of the disks and spheres (Fig. 2).

Taking the literature values for the exponent β in Eq. (4) as given quantities, that is, $\beta=0.14$ for $d_E=2$ [23], and $\beta=0.41$ for $d_E=3$ [13], the average percolation threshold values were determined as $p_c=0.37$ for $d_E=2$, and $p_c=0.080$ for $d_E=3$ [Figs. 6(a) and 6(c)]. These values are somewhat higher than the theoretical predictions, as expected for finite matrix sizes [21]. Although there is a slight variation of the fractal dimension with the percolation probability (Fig. 7), Eq. (5) can be fulfilled in a reasonable range by fits of Eq. (6) to the power law of the correlation length [Figs. 6(b) and 6(d)].

Coherent flow of fluids in the pore space of lacunar percolation systems is expected to be influenced by the constraints imposed by geometric confinements. The transport-mediating pore-space structure is called the ''percolation backbone'' with the fractal dimension d_f^b [24]. A definition is that two independent pathways to the sample edges exist at each site [24]. For more details, see [1,4,7], for instance.

The fractal dimensions of the backbone and of the whole cluster are related as [15]

$$\beta_b=\tfrac{1}{2}(\nu\, d_E+3\beta)-1, \tag{11}$$

$$d_f^b=d_E-\frac{\beta_b}{\nu}, \tag{12}$$

where β_b is the backbone-related exponent in analogy to that in Eq. (4). In the simulations of the backbone, it was assumed that singly connected pore-space channels do not contribute to transport. The results are summarized in Table I and are illustrated in Fig. 10.

V. EXPERIMENTAL RESULTS FOR THE MODEL OBJECTS

A. Black-and-white conversion of spin-density images

Figures 8(a) and 8(d) show the spin-density images of static water filled in the pore space of two- and three-dimensional swiss-cheese percolation objects, respectively. The objects were fabricated using computer-simulated clusters as templates [compare Figs. 2(a) and 2(b)]. The gray shades directly reflect the local porosity in the voxels. That is, there are not only ''pure'' matrix and ''pure'' pore-space voxels as in the case of the computer-simulated clusters. Apart from that, the water signals are unavoidably superimposed by noise in the NMR experiments. On the other hand, the visual inspection reveals a good coincidence of the simulated and the measured patterns in spite of any inaccuracies in the object fabrication.

The evaluation of the mean volume-averaged porosity [Eq. (7)] for probe-volume radii below the correlation length requires the unambiguous assignment of the pixels or voxels either to the pore space or to the matrix. The gray-scale images must therefore be converted to black-and-white contrasts. A straightforward procedure for this purpose is described in [2].

The mean volume-averaged porosity was plotted in a form similar to the data representation in Fig. 5. In this way, the parameters d_f, P_∞, and ξ can be evaluated.

B. Experimental determination of the percolation backbone

The percolation backbone can experimentally be examined by velocity mapping of water flowing through the rebuilt percolation objects. The gray-shade representation of

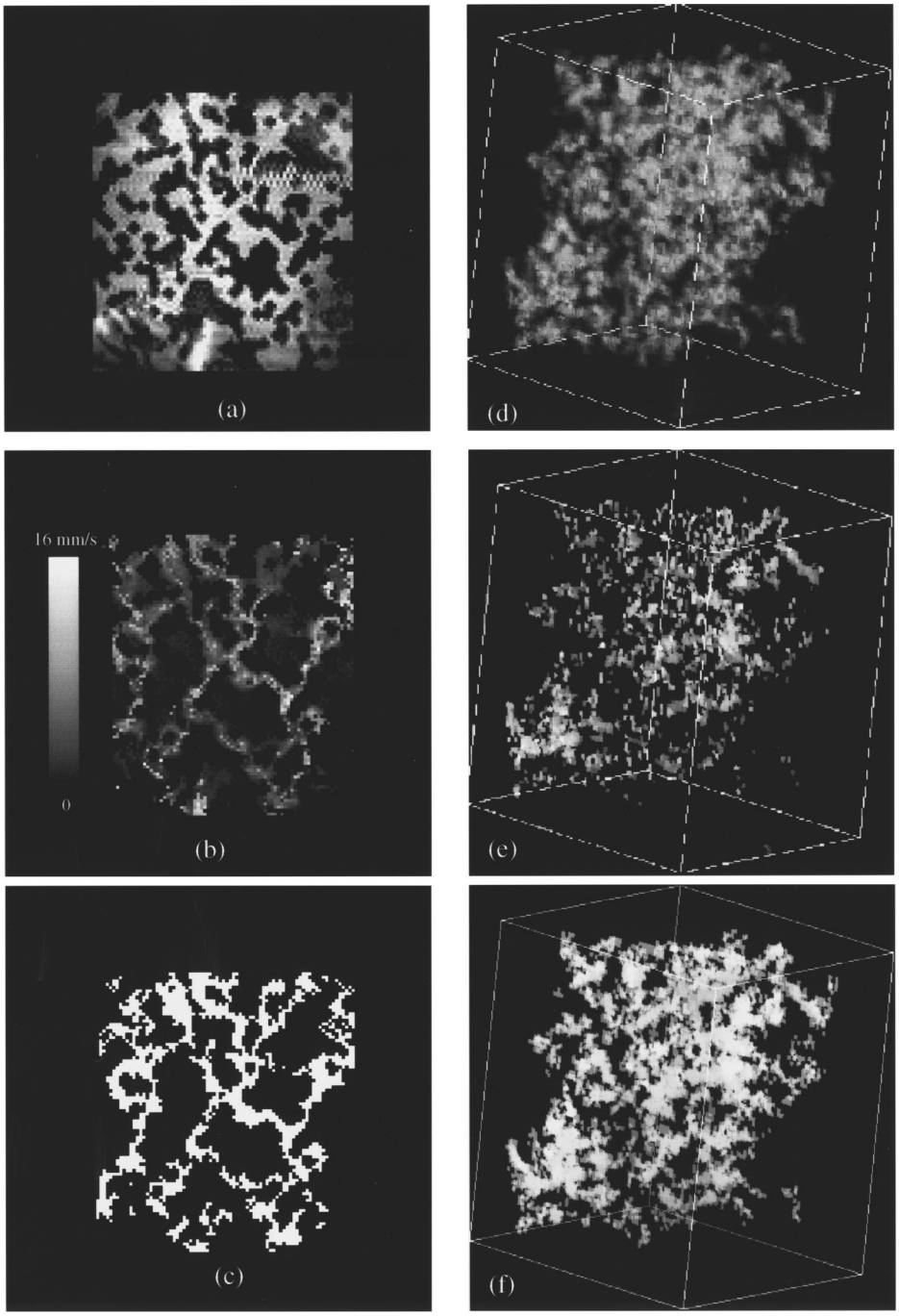

FIG. 8. Spin-density images and velocity maps of the water-filled pore space measured in two- and three-dimensional percolation objects. The digital resolution was 300 μm, the field of view 38.4 mm in each dimension. (a) Spin-density image of a water-filled two-dimensional swiss-cheese object fabricated for $p-p_c=0.087$. This object corresponds to the computer simulated pattern shown in Fig. 2(a). The gray shades arise from the local spin density. (b) Velocity map of water percolating through the object (a): The velocity magnitude is represented by gray shades. That is, the intensity is proportional to the absolute value of the velocity $v=(v_x^2+v_z^2)^{1/2}$. The preferential flow pathways along the percolation backbone are evident. (c) Two-dimensional $(d_E=2)$ black-and-white-converted representation of the backbone of (b). The velocity noise level defining the black-white threshold of the pixel representation was 0.9 mm/s. (d) Spin-density image of a water-filled three-dimensional swiss-cheese object fabricated for $p-p_c=0.0085$. This object corresponds to the computer-simulated cluster shown in Fig. 2(b). The gray shades arise partly from the local spin density and partly from the superimposed voxel projections on the drawing plane. (e) Velocity map of water flowing through the object (d). The velocity magnitude is represented by gray scales. In this case, the intensity is proportional to the absolute value of the velocity $v=(v_x^2+v_y^2+v_z^2)^{1/2}$. (f) Three-dimensional $(d_E=3)$ black-and-white-converted backbone representation of (e). The velocity noise level is the same as in (c).

the two- or three-dimensional velocity maps Figs. 8(b) and 8(e) directly visualizes the main transport pathways.

Furthermore, the two- or three-dimensional spin-density images Figs. 8(a) and 8(d) can be ''filtered'' with the aid of the corresponding velocity maps, Figs. 8(b) and 8(e). That is, all voxels with velocity magnitudes below the rms noise level in the velocity maps are converted to ''black'' in the spin-density maps. All other voxels were taken as ''white.''

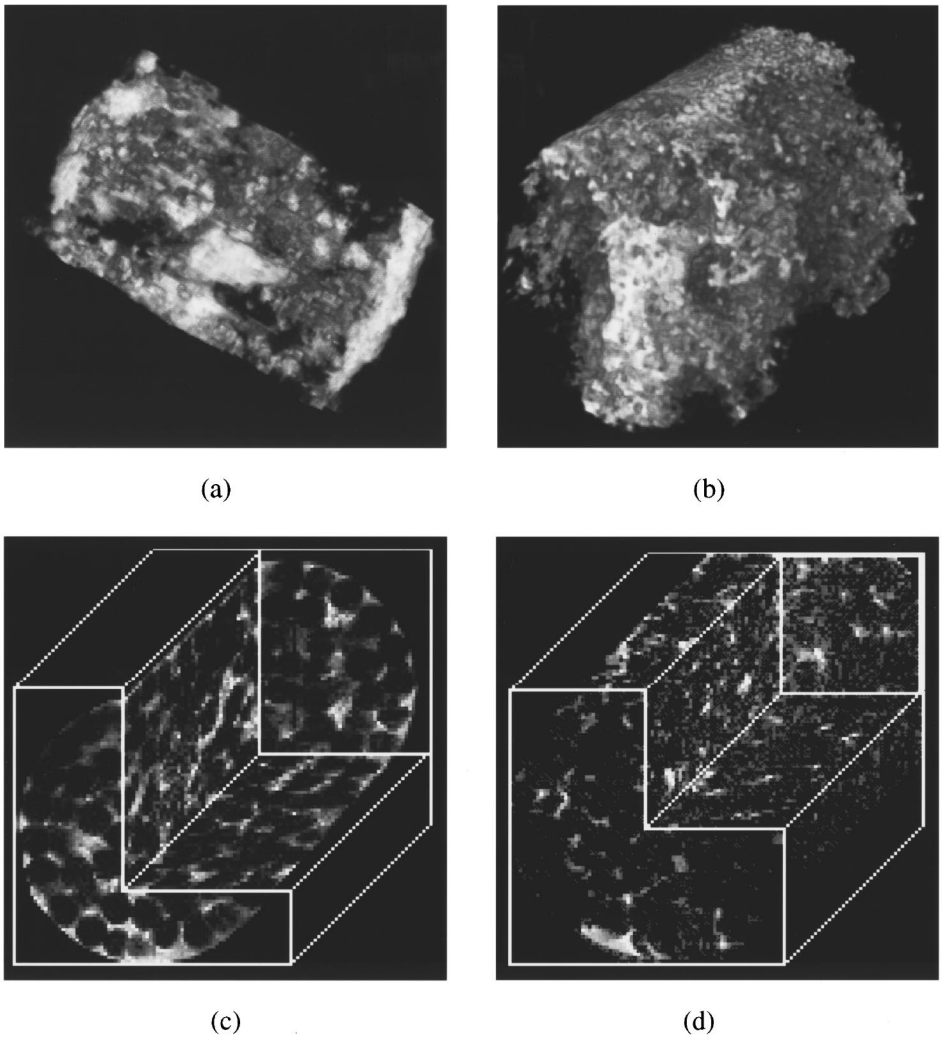

FIG. 9. Three-dimensional spin density images of water-filled natural and granular materials having a lacunar structure. (a) Pumice stone: The sample radius was 13 mm, the length was 18 mm. The image data set consists of $100\times100\times70$ voxels. The data were visualized with the aid of a ray-tracing algorithm. The voxel resolution was 250 μm. (b) Natural sea sponge: The sample radius was 4 mm, the length was 10 mm. The data set is visualized with the aid of a ray-tracing algorithm, as (a). The image data consist of $80\times80\times80$ voxels. The digital resolution was 100 μm. (c) Glass bead agglomerate: The sample radius was 4 mm, the length was 10 mm. The gray shades reflect the local spin density. In this multisectional representation merely voxels at the surfaces are displayed. The bead diameter was (1.0 ± 0.2) mm. The voxel resolution was 100 μm. (d) Quartz sand agglomerate: The sample radius was 4 mm, the length was 10 mm. The particle diameters ranged from 450 to 1000 μm. The gray shades reflect the local spin density. The voxel resolution was 100 μm. In this multisectional representation merely voxels at the surfaces are displayed.

This procedure permits the unambiguous rendering of images of the percolation backbone according to the very definition [24]. Typical results are represented by Figs. 8(c) and 8(f). The main-flow direction was along the z direction. The velocity noise level was evaluated to be in the range 0.8–0.9 mm/s. The variation of the flow rate did not significantly change the backbone structure.

TABLE II. Experimental porosity and pseudofractal dimensions of the whole pore space, d_{pf}, and of the backbone, d_{pf}^{b}, of practical lacunar systems obtained by six-dimensional NMR microscopy.

	$\overline{\rho_0}$	d_{pf}	d_{pf}^{b}
Pumice stone	0.6	2.9	2.9
Natural sponge[a]	0.8	2.9	2.9
Glass beads[a]	0.4	2.5	2.5
Quartz sand	0.3	2.7	2.7

[a]Data from [2].

The representation of the mean volume-averaged porosity of the backbone patterns as a function of the probe-volume radius permits the evaluation of the fractal dimension characterizing this reduced pore space. The results are listed in Table I. Contrary to the site percolation model, the fractal dimension of the swiss-cheese backbone is closer to that of the complete pore space. The magnitudes of the fractal dimensions are compared in Fig. 10.

VI. EXPERIMENTAL RESULTS OF PRACTICAL SYSTEMS

The objective of our work is to find an experimental protocol for the NMR characterization of pore spaces in practi-

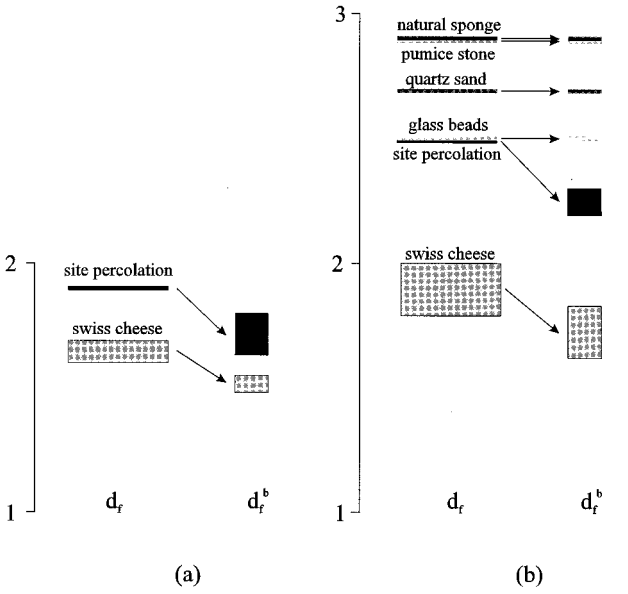

FIG. 10. Illustration of the variation of the (pseudo) fractal dimension d_f and the (pseudo) fractal dimension of the backbone d_f^b of various lacunar objects and materials as evaluated from NMR microimaging data. The fractal parameters of the random percolation clusters scatter in the indicated ranges depending on the object sample. (a) $d_E=2$. (b) $d_E=3$.

cal systems. These can be of a natural origin such as pumice or sponge, whereas granular agglomerates are of a more technical importance. A number of samples of this sort were studied in the same way as the fabricated percolation objects. In order to be able to image the pore space, the samples were evacuated and filled with water as already described in context with the fabricated objects.

A. Pumice stone

Figure 9(a) represents a NMR spin-density image of the three-dimensional distribution of static water in a pumice stone with an overall porosity of 0.6. The gray shades of this image were converted into black-and-white contrasts. Velocity maps recorded with flowing water permit the rendering of the percolation backbone. Interestingly, only a few voxels were suppressed by this ''finite velocity filtering.'' The conclusion is that almost all voxels contribute to transport by flow. That is, the pseudofractal dimension and the pseudofractal dimension of the backbone practically coincide (see Table II and Fig. 10). The pore space must be highly cross-linked so that dead ends are unlikely.

B. Natural sponge

A natural sea sponge sample was filled with water and imaged by six-dimensional NMR microscopy velocity mapping. The spin-density image recorded with static water is represented by Fig. 9(b). The overall porosity was 0.8. The evaluations show that the percolation backbone again largely coincides with the whole pore space (see Table II and Fig. 10).

C. Glass bead agglomerates

Granular systems are of actual practical interest. We have studied agglomerates of glass beads with well-defined diameters of (1.0 ± 0.2) mm. The interstitial space was filled with water and imaged in the same way as the other samples. Figure 9(c) shows a spin-density image. Obviously, the beads were packed less symmetrically as expected from the theoretical point of view. Reasons are the unavoidable distribution of the bead diameters, and constraints by the sample tube. However, the pseudofractal dimension of the black-and-white-converted spin-density image turned out to be practically the same as that of computer simulations of bcc-packed spheres [2]. In this case it is clear that the backbone coincides with the whole pore space (Table II and Fig. 10).

D. Quartz sand

As another granular system we have studied tightly packed quartz sand. The nominal diameter distribution of the grains covers a range 450–1000 μm. Figure 9(d) displays a three-dimensional spin-density image of the water-filled interstitial space. The pseudo-fractal dimension of the black-and-white-converted spin-density image again coincides with that of the percolation backbone (Table II and Fig. 10).

VII. DISCUSSION

In a first step, the swiss-cheese model was examined in more than 100 computer simulations in two dimensions, and in more than 40 in three dimensions. A suitable parameter set for the characterization of the percolation network is formed by the fractal dimension d_f, the correlation length ξ, and the percolation probability P_∞. Different lattice sizes, varied in a range from 70×70 to 1000×1000, corroborate the same parameter values.

The simulated pore-space patterns were used as templates for the fabrication of two- or three-dimensional lacunar objects. The fractal properties of these objects were studied by NMR microscopy after filling the pore spaces with water. The experimental data were evaluated in an equivalent way as the computer simulations. The procedures were tested by juxtaposing the simulated and measured results. The parameters deduced from the NMR data perfectly reproduce the parameters characterizing the computer simulations.

It was demonstrated that the percolation backbone can experimentally be separated with the aid of flow velocity maps. The fractal dimension of the backbone can be evaluated and used as a further parameter characterizing the pore space. As a result, the pore spaces of natural and practical systems tend to have coinciding (pseudo) fractal dimensions for the total pore space and the backbone part of it. This is in contrast to the random-site and swiss-cheese percolation objects.

The modeling of typical natural percolation objects requires the simulation of random percolation clusters far away from the percolation threshold $p\gg p_c$, where dead ends are unlikely. In this case, theoretical predictions for random percolation networks become unreliable. That is, the experimental parameters determined in this work for practical systems do not yet have their theoretical counterparts.

In random-site percolation clusters the backbone concerns

only a small part of the network. Close to the percolation threshold the cluster tends to consist of dead ends [1]. This property is less pronounced with continuum swiss-cheese models. Far away from the percolation threshold it becomes more and more difficult to distinguish a backbone from the total percolation cluster at all. Finally, in natural lacunar objects the backbone appears to coincide totally with the whole percolation network (compare Fig. 10). The pore space of natural lacunar objects obviously tends to be highly interconnected.

ACKNOWLEDGMENTS

We thank Jan Weis for stimulating discussions and Kay Rydyger, Hans Wiringer, and Ute Görke for assistance in the course of the experiments. One of us (R. K.) is indebted to Paul Callaghan for an excursion to Lake Taupo, New Zealand, where the pumice sample examined in this work was picked up. Financial support by the Deutsche Forschungsgemeinschaft is gratefully acknowledged.

[1] D. Stauffer and A. Aharony, *Introduction to Percolation Theory* (Taylor and Francis, London, 1985).
[2] H.-P. Müller, J. Weis, and R. Kimmich, Phys. Rev. E **52**, 5195 (1995).
[3] H.-P. Müller, R. Kimmich, and J. Weis, Magn. Reson. Imaging **74**, 955 (1996).
[4] H.-P. Müller, R. Kimmich, and J. Weis, Phys. Rev. E **54**, 5278 (1996).
[5] B. Lorenz, I. Orgzall and H.-O. Heuer, J. Phys. A **26**, 4711 (1993).
[6] I. B. Halperin, S. Feng, and P. N. Sen, Phys. Rev. Lett. **54**, 2391 (1985).
[7] M. Sahimi, *Flow and Transport in Porous Media and Fractured Rock* (VCH Verlagsgesellschaft mbH, Weinheim, 1995).
[8] S. Feng, B. I. Halperin, and P. N. Sen, Phys. Rev. B **35**, 197 (1987).
[9] B. B. Mandelbrot, *The Fractal Geometry of Nature* (Freeman and Company, New York, 1982).
[10] *Fractals in Science*, edited by A. Bunde and S. Havlin (Springer-Verlag, Berlin, 1994).
[11] R. Orbach, Science **231**, 814 (1986).
[12] A. Kapitulnik, A. Aharony, G. Deutscher, and D. Stauffer, J. Phys. A **16**, L269 (1983).
[13] W. T. Elam, A. R. Kerstein, and J. J. Rehr, Phys. Rev. Lett. **52**, 1516 (1984).
[14] *Fractals and Disordered Systems*, edited by A. Bunde and S. Havlin (Springer-Verlag, Berlin, 1991).
[15] C. Liem and N. Jan, J. Phys. A **21**, L243 (1988).
[16] J. Weis, J. Frollo, and L. Budinski, Z. Naturforsch. Teil A **44**, 1151 (1989).
[17] T. W. Redpath, D. G. Morris, R. A. Jones, and J. M. S. Hutchison, Phys. Med. Biol. **29**, 891 (1984).
[18] J. Bittoun *et al.*, Magn. Reson. Med. **29**, 674 (1990).
[19] P. T. Callaghan, *Principles of Nuclear Magnetic Resonance Microscopy* (Clarendon, Oxford, 1991).
[20] R. Kimmich, *NMR: Tomography, Diffusometry, Relaxometry* (Springer, Berlin, 1997).
[21] J. Kertész, J. Phys. Lett. **42**, L393 (1981).
[22] G. E. Pike and C. H. Seager, Phys. Rev. B **10**, 1421 (1974).
[23] E. T. Gawlinski and H. E. Stanley, J. Phys. A **14**, L291 (1981).
[24] J. Mastorakos and P. Argyrakis, Phys. Rev. E **48**, 4847 (1993).